A study of lubricant displacement under a flying head slider using an Optical Surface Analyzer

Takeshi Watanabe and David B.Bogy

Computer Mechanics Laboratory
Department of Mechanical Engineering
University of California, Berkeley, CA 94720

Abstract

Lubricant flow on a hard disk due to a dragging or flying head slider is studied using an Optical Surface Analyzer (OSA). Even when no contact occurs between the disk and slider, the lubricant flows due to various forces, e.g. centrifugal force, air shear force and air bearing pressure.

The OSA experiments confirmed that lubricant migration increased with disk rotational speed, and decreased with the ratio of bonded to mobile lubricant for the same total lubricant thickness.

The total “lubricant depletion depth” is inversely proportional to the disk rotational speed because the depletion due to air bearing pressure is restored by the centrifugal force and air shear force. The surface topography is also found to affect the lubricant depletion depth. However, the effect of the bonded ratio was small.

We also analyzed the lubricant thickness modulation along a track. It was found that lubricant pooling occurred on the lubricant depletion tracks, but there was no strong correlation between the disk topography and the lubricant modulation. Its spatial wavelength appears to correlate with the dynamic air bearing frequencies.

Keyword: Lubricant flow, Lubricant migration, Air bearing pressure, Bonded ratio, Optical surface analyzer

1.Introduction

The disk lubricant plays an important role in a magnetic disk surface. Indeed, to optimize the tribological performance of the head-disk interface, it is essential that the lubricant layer be retained uniformly on the disk surface. Even if no contact occurs between the disk and slider, lubricant flow is affected by several factors correlated with head-disk interaction. Centrifugal force, air shear flow and air bearing pressure all have significant effects on the thin lubricant films, and they may possibly cause uneven lubricant distribution. Moreover, magnetic recording density has been increasing at a rate of more than 100 percent per year. Disk rotational speed has also increased and the head flying heights have decreased at an accelerated pace. Therefore it is expected that both centrifugal and air shear force effects on the lubricant flow will become more pronounced. Consequently it is even more important to study and understand lubricant flow caused by centrifugal force, air shear flow and air bearing pressure to ensure effective disk lubrication in the near future.

Some of the issues discussed above have already been observed in a few published papers. The flow of a viscous layer over a smooth rotating disk, for example, has been studied with particular relevance to spin coating [1]. Ma *et al.* studied hard disk rotation, and concluded that the disk roughness effect prevents the lubricant from flowing freely, and that the flow rate depends on the shape of the disk roughness on the disk [2][3]. Pouwer and Kawakubo calculated the change in lubricant thickness due to centrifugal and air shear flow effects on the lubrication surface of the disk [4]. Pit *et al.* studied a lubricant “pattern” under a flying head using the OSA[5]. They called these lubricant patterns “moguls”. However, the relation between a flying head slider and lubricant flow has not yet been considered in sufficient detail for our purpose.

In this paper we first present results obtained from modeling lubricant flow and comparing them with the experimental results observed using an Optical Surface Analyzer (OSA). This was done in order to study in detail how lubricant flow is affected by centrifugal force and air shear force. Next, we examine the effects of air bearing pressure on lubricant flow, which we studied by executing long-term flyability tests. Finally, we analyze these results in order to understand lubricant flow under the flying slider rails.

2.Experiment Procedure and Set-Up

A tribology tester (TTi TriboCop), consisting of an air bearing spindle and a head mount fixture, was used to conduct long-term flyability tests. 50% (1.6mm by 2.05mm) TPC (transverse pressure contour) positive pressure sliders (as shown in Fig.2.1) were used. The disks were commercially available glass disks with 80 Å of carbon overcoat lubricated by a dipping process with Fomblin Z-DOL (MW = 6000). The long-term flyability tests were conducted as follows. We began by mounting the disk on the air bearing spindle of the tribology tester and bringing the rotational speed up to a stable RPM level. Next, the slider was positioned at an inner radius track on the disk, then allowed to move to a radius of about 28mm. Then, the head continued to fly on the same track throughout the experiment. After the long-term flyability test (generally 24 hours), the head was returned to the inner radius track. Then the head was unloaded off the disk and the disk rotation was stopped. Finally, the disk surface was observed using an OSA (Candela TS-2100). The OSA is an optical measurement instrument designed to detect carbon wear, lubricant wear, lubricant depletion, lubricant accumulation, surface roughness, and lubricant decomposition on carbon coated thin film disks [6]. The thickness resolution of the OSA is less than 1 Å.

3.Results and Discussion

3.1 The effect of centrifugal and air shear forces on lubricant flow

3.1.1 Comparison of the simulation with experimental results

Before starting the long-term flyability test, a long-term disk rotational test (without the flying head slider) was carried out, and a numerical simulation was performed for a rotational speed of 10,000 RPM in order to understand the effect of the centrifugal and the air shear forces on the lubricant flow. Two types of disks were employed in this experiment, as shown in Table.3.1.1. The only differences between the two were the initial lubricant thickness and the duration of the test.

Lubricant	Sample-A	Sample-B
Type	Z-dol (MW=6000)	Z-dol (MW=6000)
Initial thickness[Å]	15	20
Bonded ratio[%]	30	30
Disk rotational time[hour]	36	103

Table.3.1.1 The disk samples

The numerical simulation flow model is [1]-[4].

$$-\rho\omega^2 r = \eta \frac{\partial^2 v_r}{\partial z^2} \qquad (1)$$

$$v_r = 0 \qquad (\text{at} \quad Z = 0) \quad (2)$$

$$\eta \frac{\partial v_r}{\partial z} = \tau_r \qquad (\text{at} \quad Z = h) \quad (3)$$

$$\tau_r = \frac{1}{2}\omega^{\frac{3}{2}} \rho_a^{\frac{1}{2}} \upsilon_a r \qquad (4)$$

where ρ is the lubricant density, η is the viscosity coefficient, ω is the disk rotational frequency, V_r is air flow velocity in the radial direction, τ_r is the air shear force on the lubricant free surface, υ_a is the kinetic viscosity coefficient and ρ_a is the air density.

Equation (1) was derived from the force balance between the viscosity term of the NS (Navier-Stokes) equation and the centrifugal force due to disk rotation, assuming that the lubricant flows in the radial direction (as shown in Fig.2.2) [7].

The numerical simulation was performed by solving equation (1) with the finite difference method. The velocity at the disk surface (Z=0) is zero because of the no-slip condition (equation (2)). Equation (4) represents the shear force on the lubricant free surface due to the air shear in the outward direction, and it is used in equation (3). The possibility of bonding between the lubricant and carbon layers was not considered in this model, and therefore the lubricant bonded ratio is assumed to be 0 % in this simulation.

Figures 3.1.1 - 3.1.2 (sample A) and Figs. 3.1.3 - 3.1.4 (sample B) illustrate the lubricant migration results. The experimental results obtained by OSA measurement are shown as a series of dots, and the simulation results are shown as lines. Figure 3.1.1 shows the sample “A” experimental and simulation results, assuming that the initial lubricant thickness was 15 Å. Figure 3.1.2 illustrates the experimental result and the simulation results, assuming that the initial lubricant thickness was 10.5 Å (= initial thickness of 15 Å – bonded thickness of 4.5 Å). Figure 3.1.3 illustrates the sample “B” experimental and simulation results assuming that the initial lubricant thickness was 20 Å. Likewise, Fig. 3.1.4 shows the experimental result and the simulation result assuming the initial lubricant thickness was 14 Å (= initial thickness of 20 Å – bonded thickness of 6 Å).

From both Figs. 3.1.1 and 3.1.3 we see that the experimental results were not consistent with the simulation results. However, the simulation profiles appear to be close to the experimental results for Figs. 3.1.2 and 3.1.4. From this we conclude that the bonded lubricant is not able to migrate, rather, it is fixed, like “a portion of the carbon layer”. Therefore, a more realistic simulation can be performed by ignoring the bonded lubricant thickness.

3.1.2 Simulation analysis for each factor

Using the above model, a numerical simulation was carried out in order to compare the centrifugal force effect with the air shear force effect on lubricant migration. Figure 3.1.5 shows the comparison between the combined “centrifugal and air shear force effects” and “the centrifugal force effect” alone.

The lubricant was Fomblin Z-03 (un-bonded). The initial thickness was 10nm, the disk rotational speed was 10,000rpm, for a duration of 100 hours. For the boundary condition, the inner velocity was set equal to zero and outer one was stress free. For the “centrifugal force effect alone” case, as shown in Fig. 3.1.5, about half of the lubricant still remained on the disk surface. However, most of the lubricant was no longer on the surface for the case of the combined “centrifugal and air shear forces”.

In Fig.3.1.6, the ratio shows the percentage of the “Amount of lubricant flow only due to Centrifugal force” compared with the total of the “Amount of lubricant flow due to combined centrifugal and air shear force”, which was derived from the results shown in Fig. 3.1.5 (i.e. Ratio(%) = (B/A) as shown in Fig.3.1.5).

In Fig. 3.1.6, the rate of lubricant flow due to centrifugal force appears to depend on the radial position, with an average of 41.8% over the entire disk surface. This ratio is certainly not negligible. Therefore, both of the force effects should be considered as important factors in the migration of the lubricant.

3.2 The effect of air bearing pressure on lubricant flow

After the long-term (24hours) flyability test, the disk surface was measured using the OSA. Figure 3.2.1 shows the circular image of the track left after such a test. Figure 3.2.2 shows a distorted Cartesian image, in which the area is the same as that in Fig. 3.2.1. The images in both Figs. 3.2.1 and 3.2.2 were measured using the phase shift mode, which is sensitive to changes in lubricant thickness. In Fig. 3.2.2, two traces are clearly seen on the disk surface. Their positions are consistent with the track location under the flying slider, which shows that the lubricant can be moved due to the air bearing pressure without contact since no contact was detected.

Figure 3.2.3 shows a cross section of the change in the lubricant thickness after the long-term flyability test. There are two negative peaks clearly visible on the lubricant surface, which indicates that lubricant depletion occurred there. To estimate the effect on the lubricant flow caused by the air bearing pressure, we measured the lubricant depletion depth as indicated in Fig. 3.2.3.

3.2.1 The correlation between disk rotational speed and lubricant depletion depth

Figures 3.2.4 - 3.2.6 show the lubricant depletion images for the disk rotational speeds of 10000, 7200 and 5400 rpm, respectively. Judging from these images, the bright lines appear to depend on the rotational speed. The lubricant depletion depth (see Fig. 3.2.3) was measured from a cross section of these images, and the values are shown in Fig. 3.2.7, where the points indicate the average of the two negative peaks under the two rails. According to this result, the lubricant depletion depth clearly decreases with the disk rotational speed.

It is conceivable that this phenomenon actually depends on the lubricant flow due to the centrifugal and the air shear forces. Since these factors are in proportion to disk speed, lubricant restoration rate would be faster at high rotational speeds than at low speeds.

3.2.2 The correlation between disk roughness and lubricant depletion depth

Figure 3.2.5 shows the lubricant depletion image for an un-textured disk, whereas Fig. 3.2.8 indicates the image for a textured disk rotating at 7200 rpm.

The difference between the lubricant depletion depth on the un-textured disk and on the textured disk is shown in Fig. 3.2.9. It is seen that the lubricant depletion depth on the textured disk is less than that on the un-textured disk. According to the published literature, the roughness on the disk surface plays a role in preventing the lubricant from migrating [2][3]. Our results indicate that the shape of the disk surface affects not only lubricant migration, but also the lubricant depletion depth under the slider. The difference in the depletion depths is primarily due to the texture, and was less than 1Å.

3.2.3 The relationship between the lubricant bond ratio and the lubricant depletion depth

For this test, we prepared two types of bonded ratio samples: 20% and 70% bonded. The experimental results indicate that the effect of the bonded ratio on the lubricant depletion depth was small, as shown in Fig. 3.2.10.

Figure 3.2.11 shows one possible explanation for the phenomenon. If the lubricant layer is bonded to the carbon layer, then the lubricant layer cannot flow in the radial direction, as discussed in section 3.1.1. On the other hand, the air bearing pressure influences the thickness of the lubricant layer locally, so the lubricant layer is not moved horizontally but may be “dented”. It is possible that this phenomenon deforms the backbone of the lubricant structure, as shown in Fig. 3.2.11, which would account for the fact that a similar lubricant depletion depth was observed regardless of the bond ratio.

3.2.4 Restoration of the lubricant layer after a long-term flyability test

The amount of lubricant flow is very small even if it is caused by air bearing pressure, and therefore it can be restored easily. Figure 3.2.12 shows the disk surface immediately after the long-term flyability test, and Fig. 3.2.13 shows the same disk 75 hours after the test. The process of lubricant restoration is shown in Fig. 3.2.14. In this case, air bearing pressure caused the lubricant to move by several angstroms. However, it could be restored to less than 1 angstrom if left for 75 hours. This shows that the observed phenomenon was related only to the lubricant flow.

3.3 Analysis of lubricant modulation under the flying head slider

3.3.1 FFT analysis of lubricant modulation

It is expected that the air bearing pressure could move the lubricant in the radial direction. However, the experimental results show that the lubricant flow occurred not only in the radial direction, but also in the circumferential direction.

Figure 3.3.1 shows an example of the OSA image after a long-term flyability test. Two traces are visible in this figure consistent with the rails of the flying head slider. Figure 3.3.2 shows the magnified image of position “A” in Fig. 3.3.1. A lubricant “modulation” is observed in this area. In fact, similar modulations were observed in most tests. Therefore, we used FFT (Fast Fourier Transform) analysis to better understand this phenomenon. We measured un-textured disks at three disk rotational speeds (10000, 7200, 5400 rpm) and a textured disk at 7200 rpm. The results are shown in Figs. 3.3.3 - 3.3.18.

For these figures, in each case the upper left graph shows the FFT analysis for the inner track, and the upper right graph shows that for the outer one. These results were obtained by calculating the FFT of the full circle (360 deg). The lower graphs on each page show the results obtained by dividing the full circle into eight parts and analyzing each separately (i.e., each area shows a 45° region).

In the 10,000 rpm case, there was no remarkable peak regardless of the track position, as shown in Figs. 3.3.3 and 3.3.4. However, a partial peak at 20-40 KHz was observed, as shown at position “B” in Fig. 3.3.5, and also at position “C” in Fig. 3.3.6. These results indicate that the lubricant modulation might be periodic and affect only a limited area.

If this lubricant modulation was caused by the performance of a flying head slider, such as flying height modulation, the entire track should have been affected. But the clearly affected area was limited, and therefore there is a possibility that this lubricant phenomenon was related to a disk surface factor.

3.3.2 Topography analysis under lubricant modulation

After the long-term flyability test (70 hours), the disk surfaces were examined, as shown in Fig. 3.3.19. Positions “D” and “E” under the flying head slider were also observed in detail using the OSA, in order to understand the correlation between disk topography and lubricant flow. The results from position “D” are shown in Fig. 3.3.20, and those from position “E” in Fig. 3.3.21. The upper images in Fig. 3.3.20 show the phase shift image of position “D” (left), and a cross section of the phase shift image (right), taken along the line indicated by the dashed arrow. The lower images show a topography image (left) and cross section of that image (right) as indicated by the dashed arrow. A dark spot is clearly seen in the phase shift image, which means that lubricant pooling occurred in this track under the flying head slider. However, there is no corresponding signal there in the topography image.

The upper left image in Fig. 3.3.21 shows a phase shift image of position “E”, and two cross sections of this area are shown as the right and lower graphs. A dark spot is also seen in this phase shift image, but again there is no corresponding signal there in the topography image.

According to these results, it is obvious that a lubricant pooling area exists on the lubricant depletion tracks. However, we were unable to prove any correlation between the lubricant pooling and the disk topography in this investigation. Therefore, this phenomenon may be related to other factors, such as the lubricant restoration ratio (viscosity coefficient), or disk topography smaller than 5 μm (the lateral resolution of our equipment was about 5 μm).

In addition, the head flying height used in these tests was above 100 nm for all test cases. Therefore, if the flying height is lower, as is the case for current commercial products, there is a possibility that clearer lubricant modulation may occur under the flying head slider. Future studies will be directed toward lower flying heights.

4. Summary

In this study, we investigated how lubricant migration is affected by centrifugal force and air shear force. To this end, we calculated the lubricant flow using a model and compared it with the experimental results observed by an OSA. In summation:

- Bonded lubricant is not able to migrate because it is fixed, as if it were a portion of the carbon layer. An approximate simulation can be performed by simply ignoring the thickness of the bonded lubricant.
- The ratio shows the percentage of the “Amount of lubricant flow due only to centrifugal force” to the “Amount of lubricant flow due to combined centrifugal and air shear force” was 41.8% on disk surface. Both the centrifugal and air shear force effects should be considered as important factors in lubricant migration.

The effects of centrifugal and air shear forces along with the air bearing pressure were also considered experimentally using a long-term flyability test. In summary:

- The lubricant can be moved by air bearing pressure.
- The lubricant depletion depth is inversely proportional to the disk rotational speed because of lubricant restoration effect due to the centrifugal and the air shear forces.
- The disk surface topography affects not only the lubricant migration but also the lubricant depletion depth due to the air bearing pressure.
- The air bearing pressure influences the lubricant layer thickness locally, so that the lubricant layer can be dented, but not moved. It is presumed that this phenomenon affects the backbone of the lubricant structure.
- The lubricant depletion can be restored, which is proof that this change was related only to the lubricant flow.

With regard to the FFT analysis under the flying head slider, our conclusions are:

- The lubricant modulation is periodic in a limited area. This modulation might not occur evenly on the disk surface.
- A lubricant pooling area exists on the lubricant depletion tracks, but no strong correlation was found between disk topography and lubricant pooling.
- Lubricant modulation may be related to other factors, such as the lubricant restoration ratio (viscosity coefficient), or disk micro-topography below 5 μm.
- The head flying height used in these tests was above 100 nm for all test cases, so there is a possibility that clearer lubricant modulation may occur under the flying head slider if the flying height is lower, as is true for current commercial products.

References

[1] Stanley Middleman, “The effect of induced air-flow on the spin coating of viscous liquids,” J. Appl. Phys. Vol. 62, No. 6, pp 2530-2532, Sep 15 (1987)

[2] F. Ma and J. Hwang, “Surface Roughness and Lubricant Depletion on a Magnetic Storage Disk,” J. Tribology, Vol. 112, pp 165-168, Jan (1990)

[3] J. S.Kim, S. Kim, and F. Ma, “Topographic effect of surface roughness on thin-film flow,” J. Appl. Phys. Vol. 73, No. 1, pp 422-428, Jan 1 (1993)

[4] Y. Kawakubo, A. Pouwer and R. Tsuchiyama, “Lubricant Flow under a Flying Head on a Thin-Film Disk,” Abstracts AP-07, pp 52-53, The 8th Joint MMM-Intermag Conference, San Antonio, TX, Jan 7-11 (2001)

[5] R.Pit, B. Marchon, S. Meeks and V.Velidandla, “Formation of Lubricant “Moguls” at Head/Dsik Interface,” Tribology letters, Vol. 10(N3), pp 133-142, Apr (2001)

[6] S. Meeks, W. Weresin and H. Rosen, “Optical Surface Analysis of the Head-Disk-Interface of Thin Film Disks,” Transactions of the ASME, Vol. 117, pp 112-118, Jan (1995)

[7] B. Bhushan and Z. Zhao, “Macroscale and Microscale Tribological Studies of Molecularly Thick Boundary Layers of Perfluoropolyether Lubricants for Magnetic Thin-Film Rigid Disks,” J. Info. Storage Proc. Syst.,Vol. 1, pp 1-21 (1999)

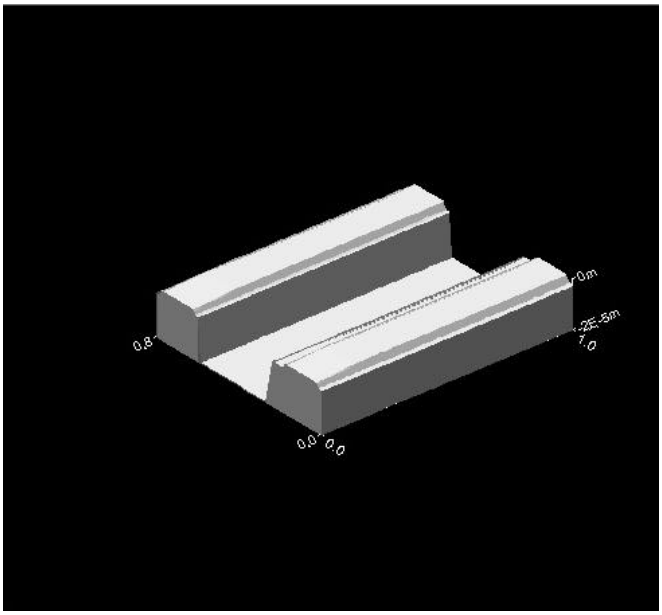

Fig. 2.1 50% TPC (transverse pressure contour) positive pressure sliders

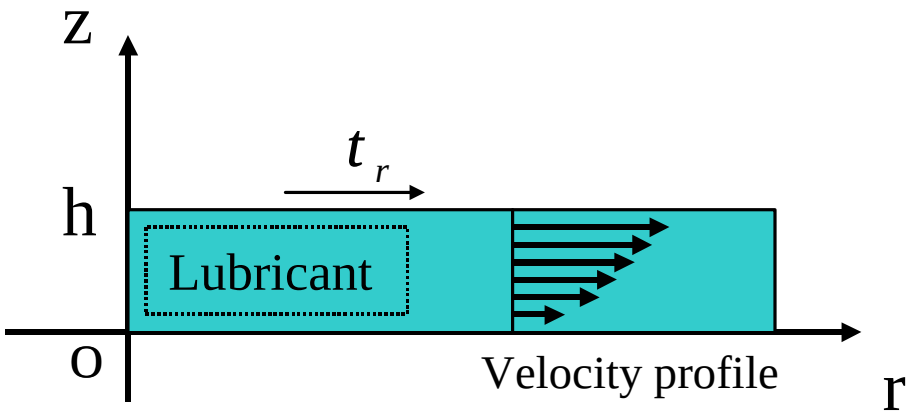

Fig. 2.2 The numerical simulation model

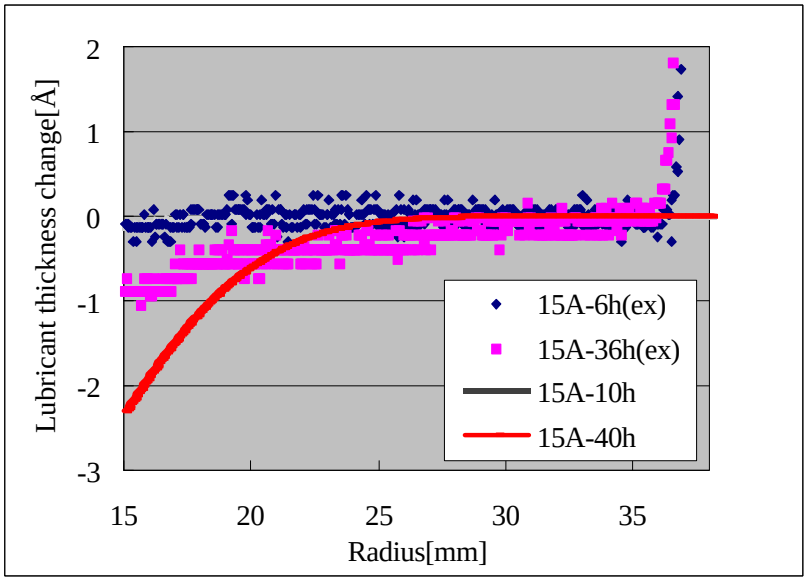

Fig. 3.1.1 Lubricant thickness change after a long-term rotational test (sample A) assuming that initial lubricant thickness is 15 Å.

Simulation results are indicated by an unbroken line. Experimental results are represented by individual dots.

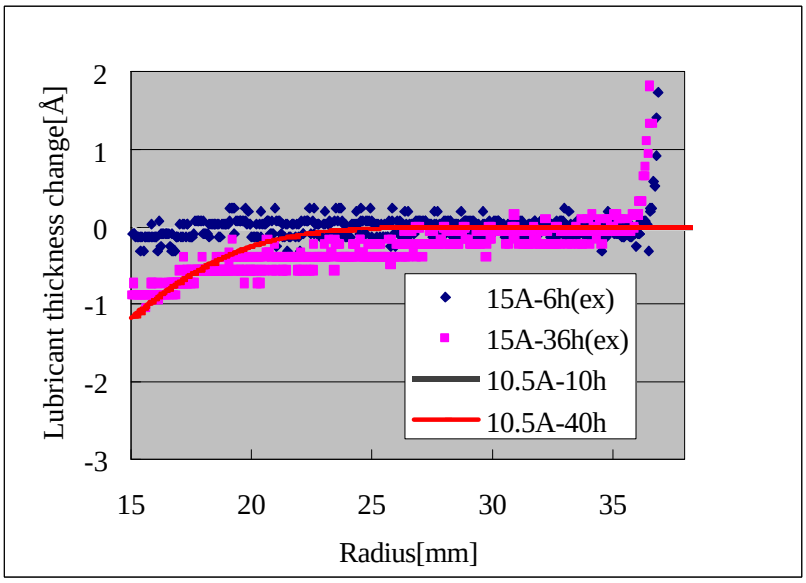

Fig. 3.1.2 Lubricant thickness change after a long-term rotational test (sample A) assuming that initial lubricant thickness is 10.5 Å.

Simulation results are indicated by unbroken lines. Experimental results are represented by individual dots.

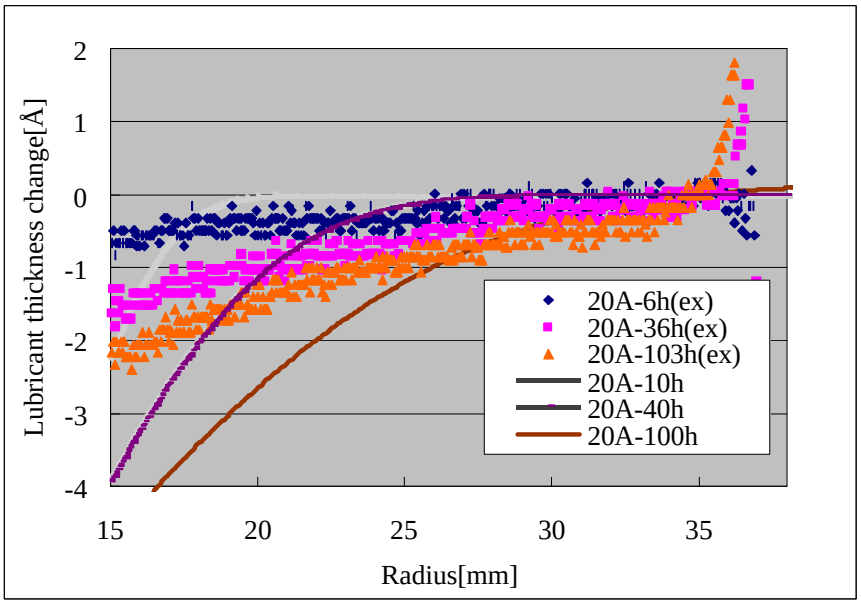

Fig. 3.1.3 Lubricant thickness change after a long-term rotational test (sample B) assuming that initial lubricant thickness is 20 Å.

Simulation results are indicated by unbroken lines. Experimental results are represented by individual dots.

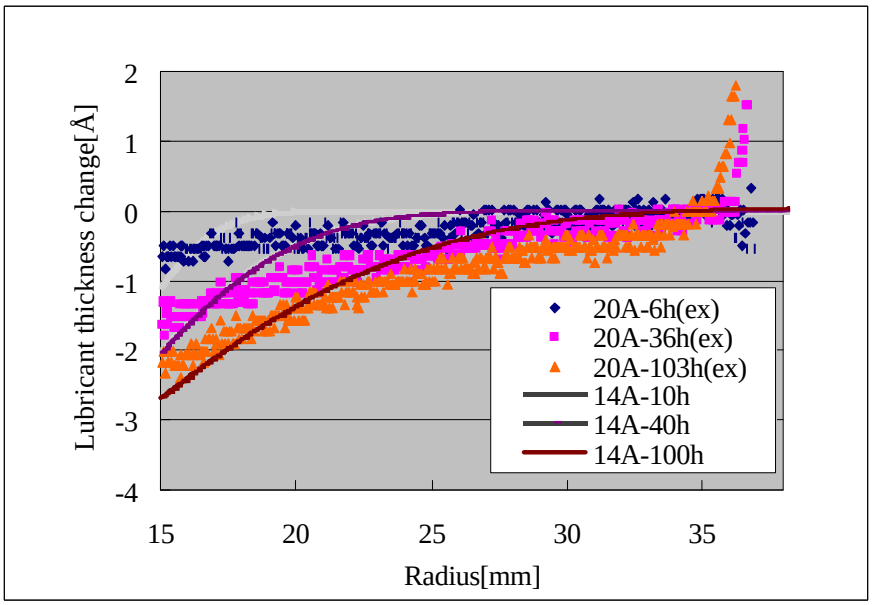

Fig. 3.1.4 lubricant thickness change after a long-term rotational test (sample B) assuming that initial lubricant thickness is 14 Å.

Simulation results are indicated by unbroken lines. Experimental results are represented by individual dots.

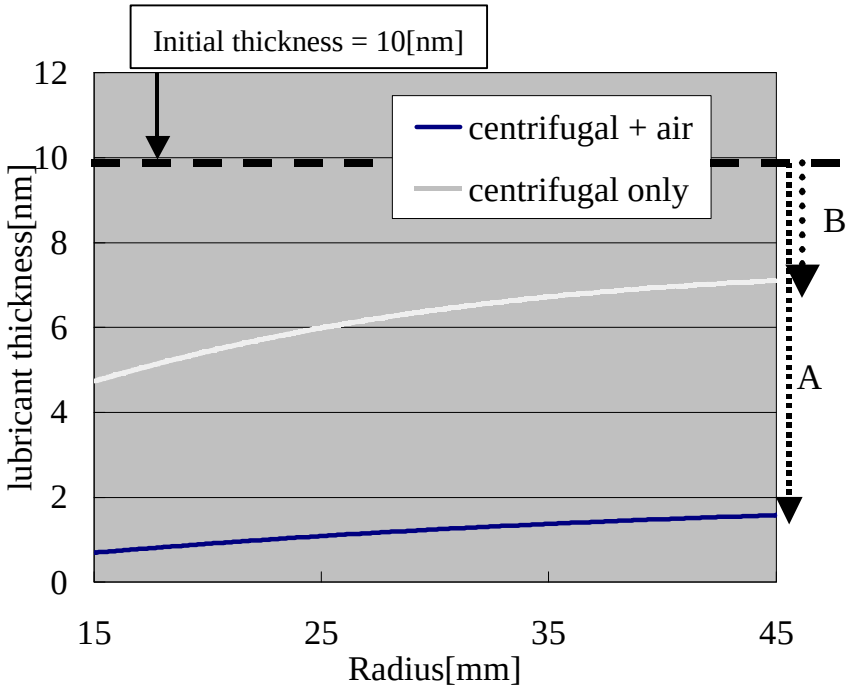

Fig. 3.1.5 Simulation of retained lubricant thickness profile after 100 hours disk rotation between "the combined centrifugal and air shear force effects" and "centrifugal force effect only."

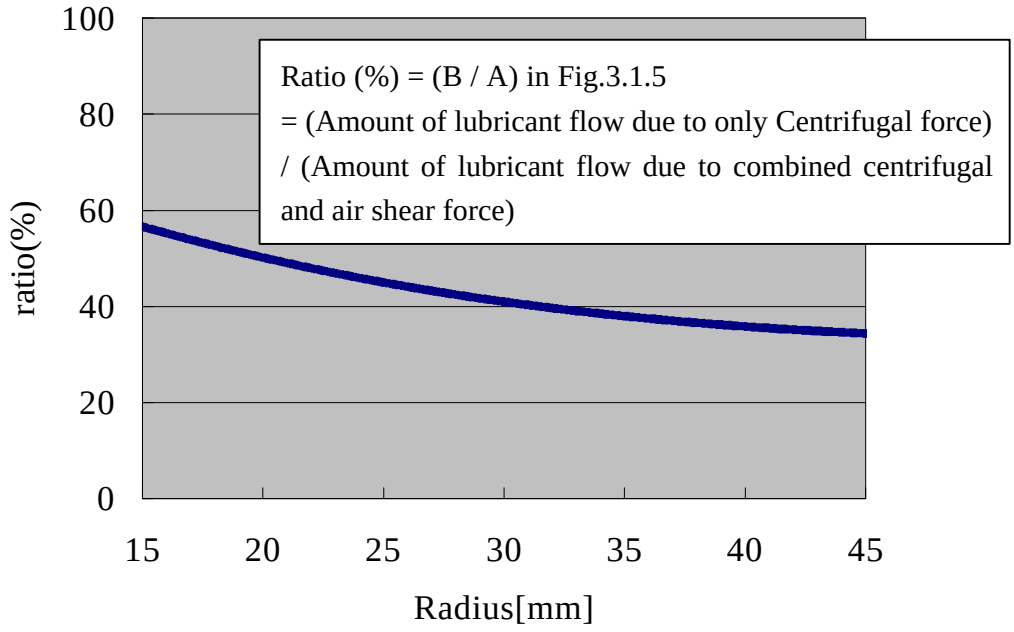

Fig. 3.1.6 Simulation of the ratio of centrifugal force effect to the combined force effects on lubricant migration after 100 hours disk rotation.

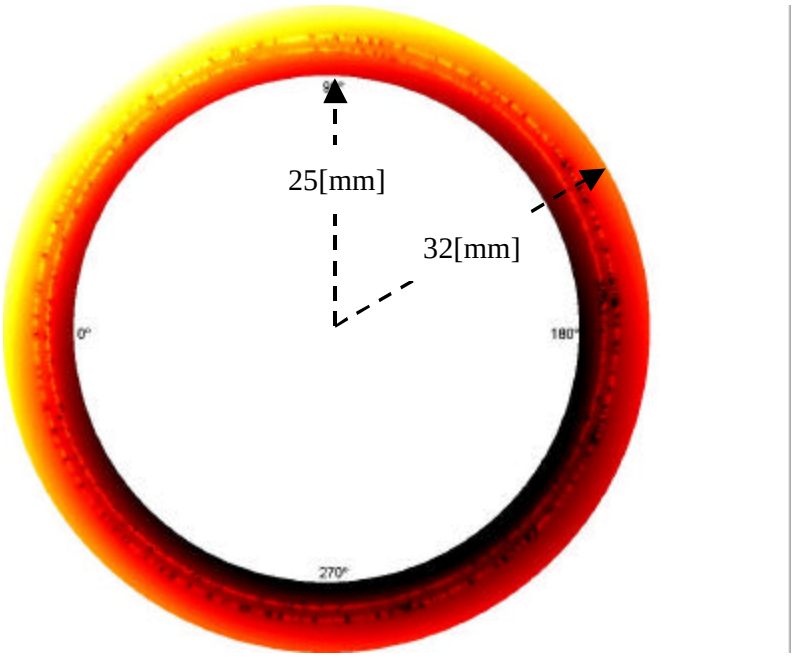

Fig. 3.2.1 OSA image (circle) after the long-term flyability test

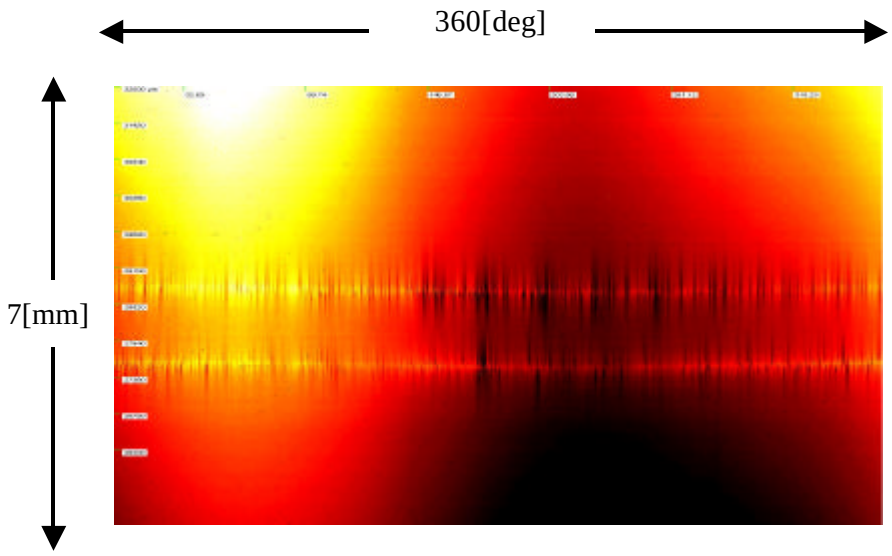

Fig. 3.2.2 OSA image (square) after the long-term flyability test
(same area as Fig. 3.2.1)

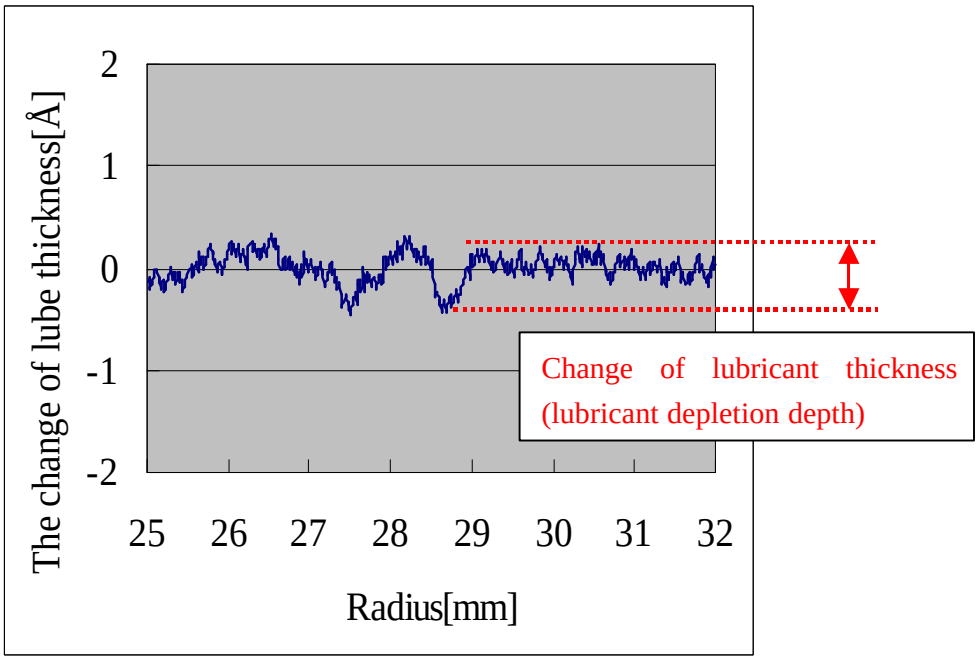

Fig. 3.2.3 Cross section showing the change in lubricant thickness after the long-term flyability test

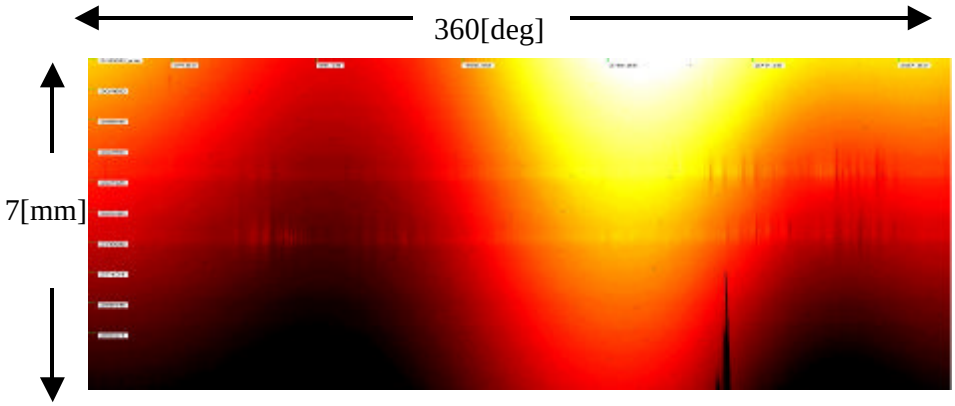

Fig. 3.2.4 OSA image after the long-term flyability test at 10,000 rpm

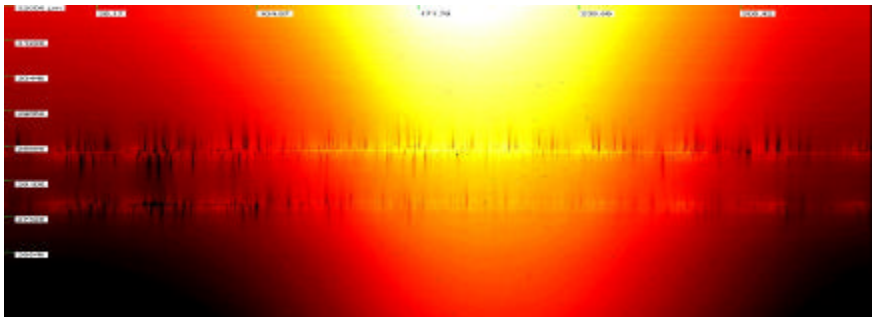

Fig. 3.2.5 OSA image after the long-term flyability test at 7200 rpm

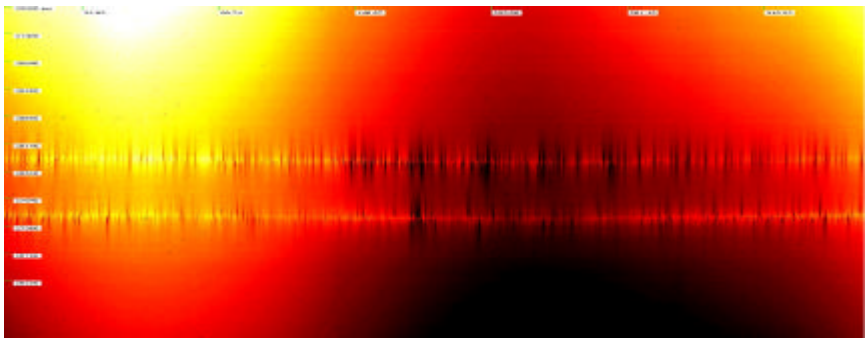

Fig. 3.2.6 OSA image after the long-term flyability test at 5400 rpm

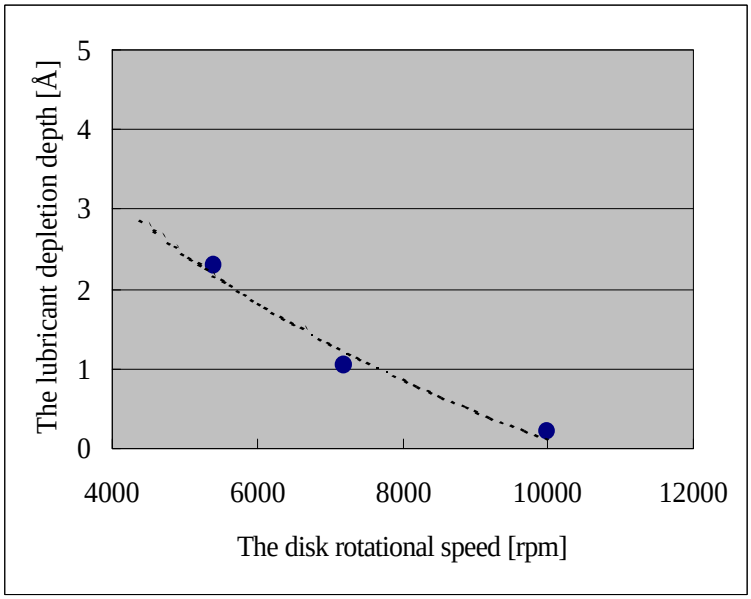

Fig. 3.2.7 The correlation between the disk rotational speed and the lubricant depletion depth (on the Un-textured disk)

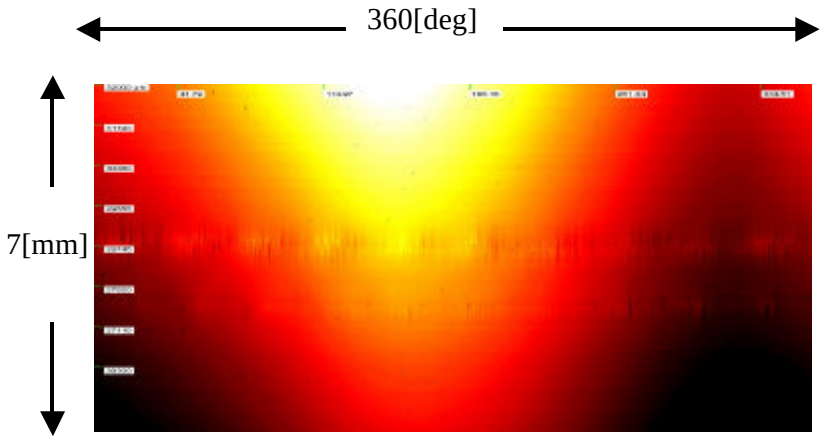

Fig. 3.2.8 Lubricant depletion image of the textured disk
(The disk rotational speed is 7200 rpm)

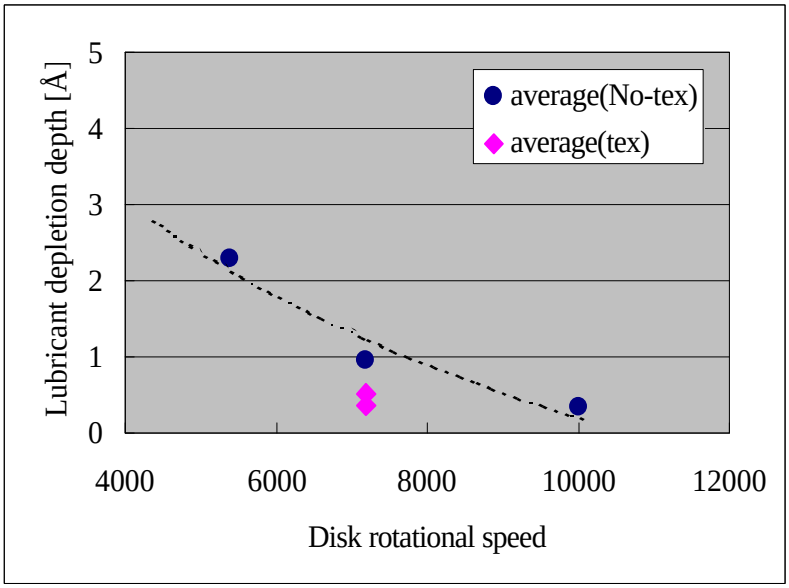

Fig. 3.2.9 Comparison of the lubricant depletion depth for un-textured vs. textured disks.

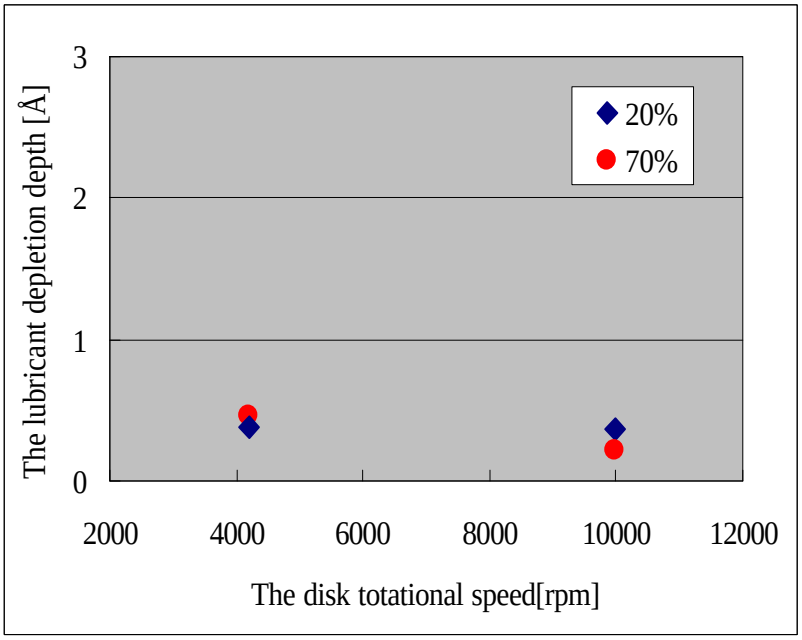

Fig. 3.2.10 Lubricant depletion depth due to the difference in the lubricant bonded ratio (initial lubricant thickness = 15 Å at 10000 rpm, 12.5 Å at 4200 rpm)

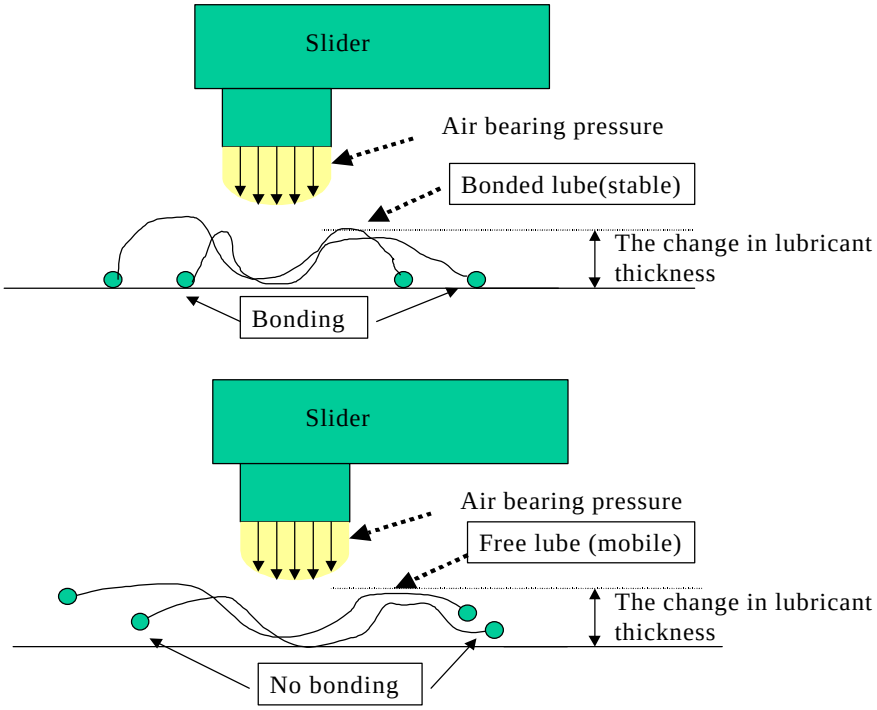

Fig. 3.2.11 A possible explanation for the results shown in Fig.3.2.10
(upper image) The air bearing effect on the bonded lubricant surface
(lower image) The air bearing effect on the free lubricant surface

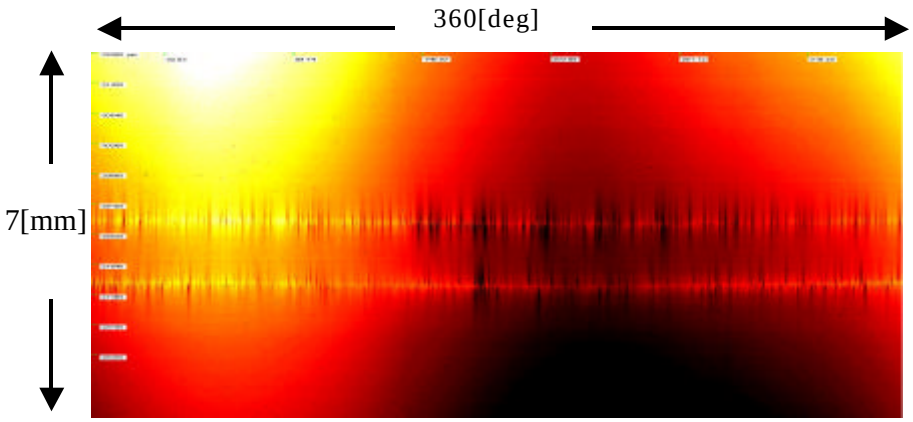

Fig. 3.2.12 Lubricant profile immediately after the long-term flyability test

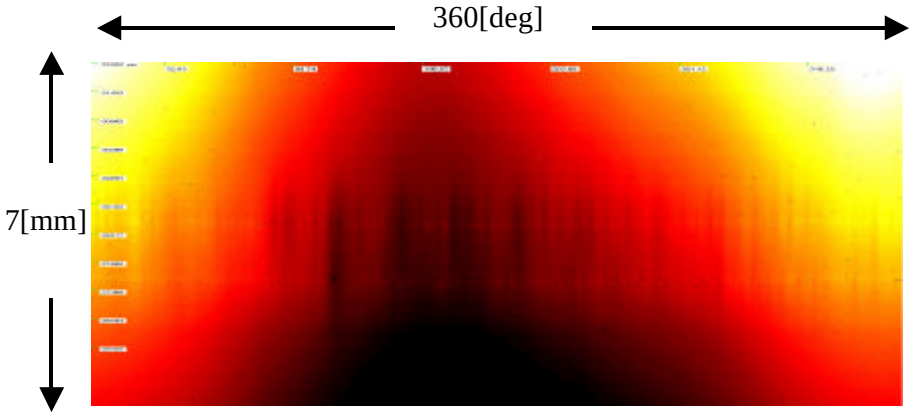

Fig. 3.2.13 Lubricant profile 75 hours after the long-term flyability test

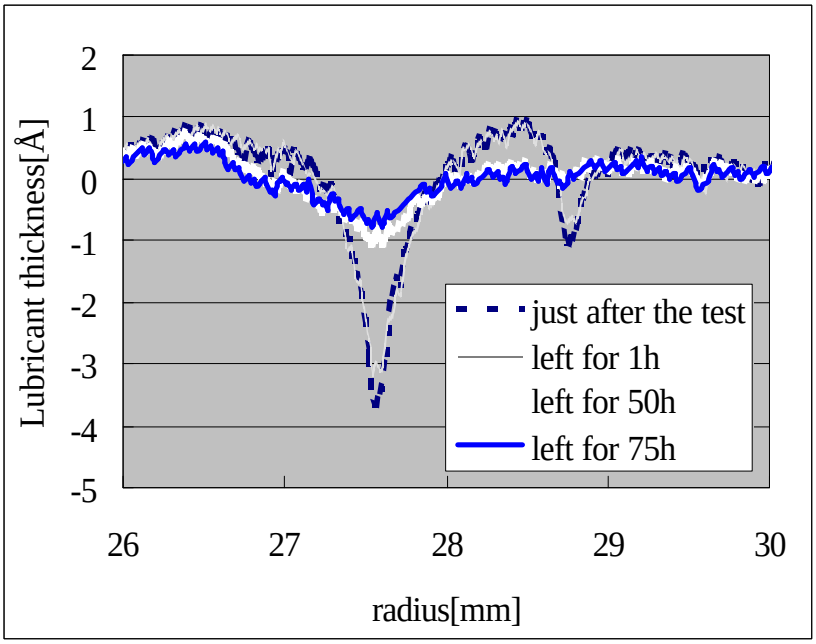

Fig. 3.2.14 The process of lubricant restoration over 75 hours

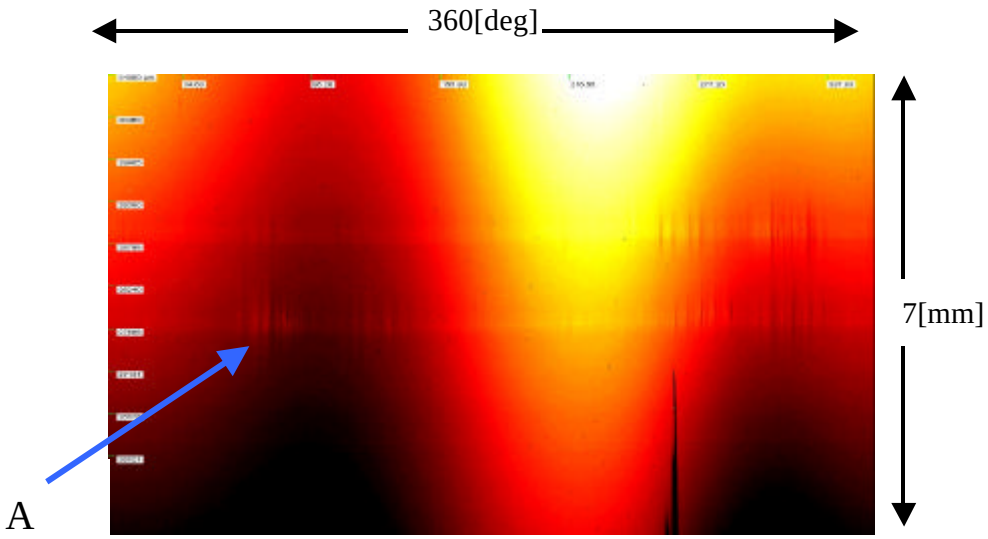

Fig. 3.3.1 OSA image after a long-term flyability test (24 hours)

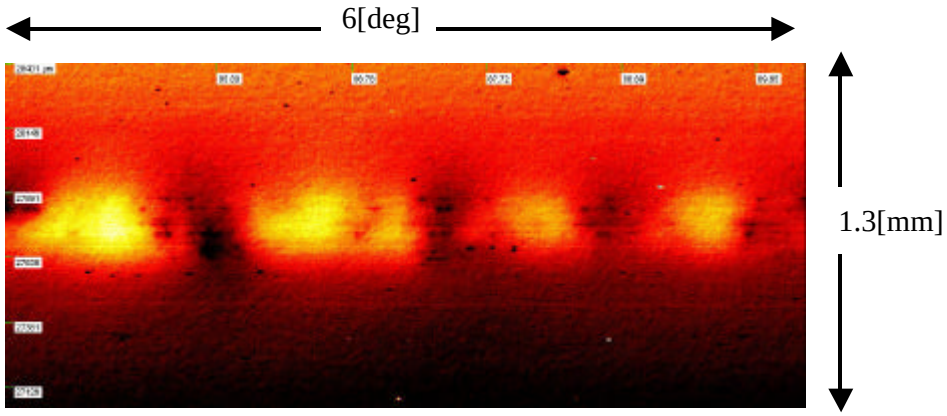

Fig. 3.3.2 Magnified image of position “A” in Fig. 3.3.1

[Un-textured disk at 10,000rpm]

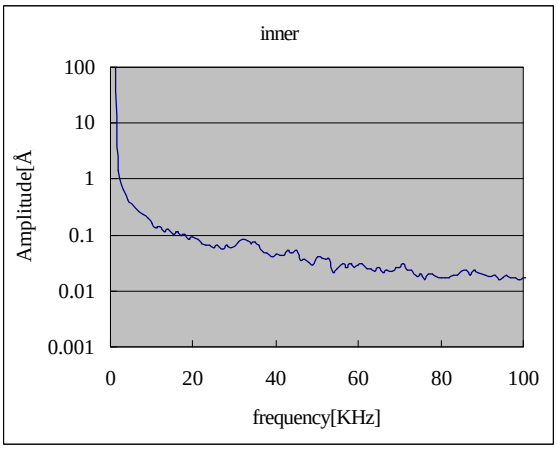

Fig. 3.3.3 FFT analysis of inner line modulation for the full circle.

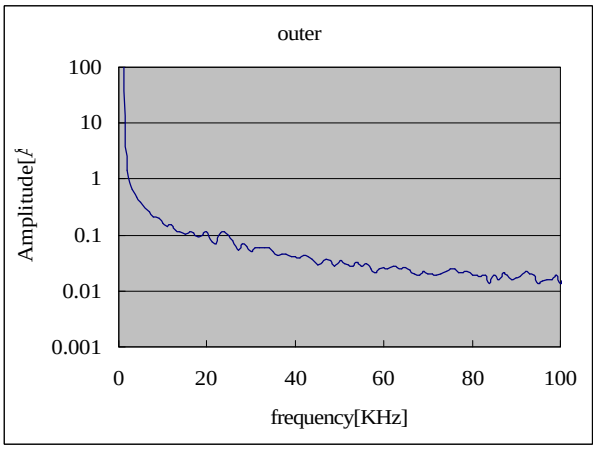

Fig. 3.3.4 FFT analysis of outer line modulation for the full circle.

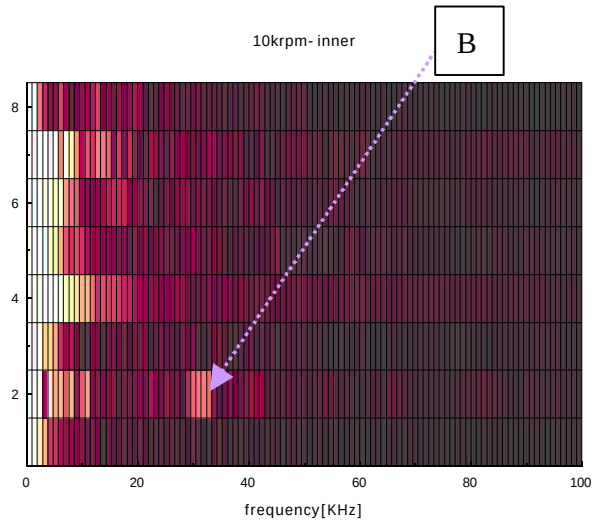

Fig. 3.3.5 FFT analysis of inner line modulation for each 45 deg segment.

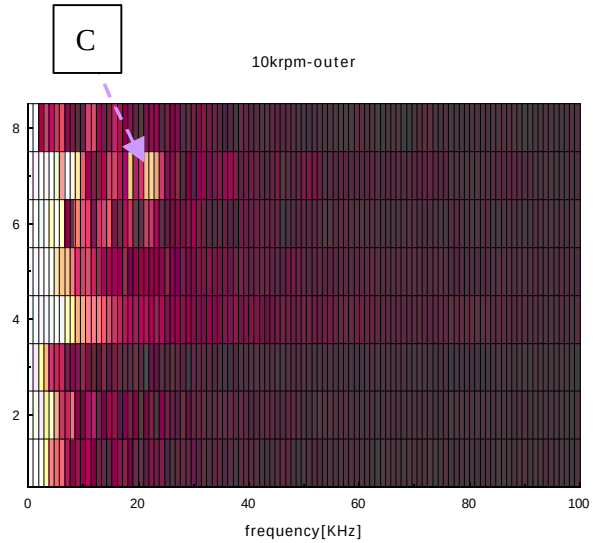

Fig. 3.3.6 FFT analysis of outer line modulation for each 45 deg segment.

[Un-textured disk at 7200rpm]

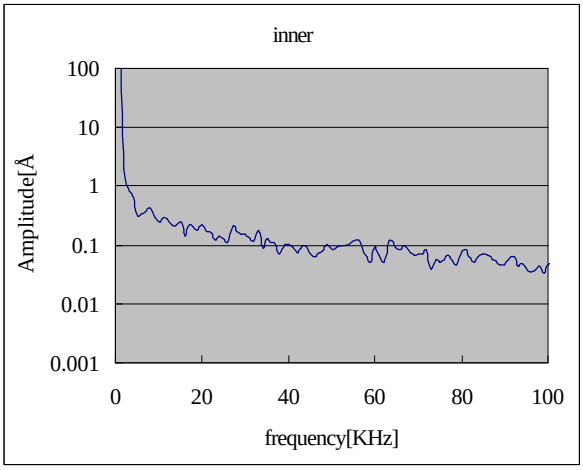

Fig. 3.3.7 FFT analysis of inner line modulation for the full circle.

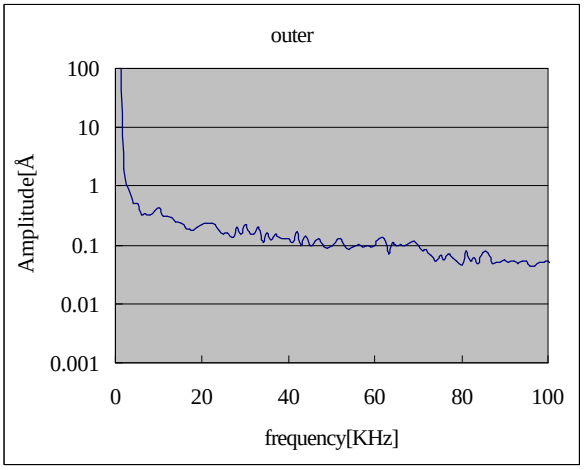

Fig. 3.3.8 FFT analysis of outer line modulation for the full circle.

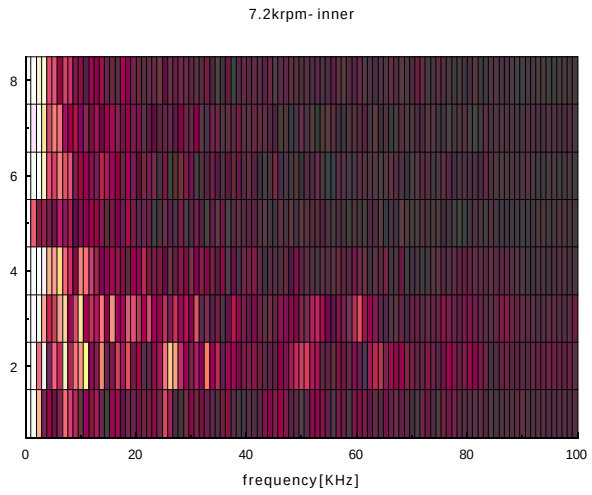

Fig. 3.3.9 FFT analysis of inner line modulation for each 45 deg segment.

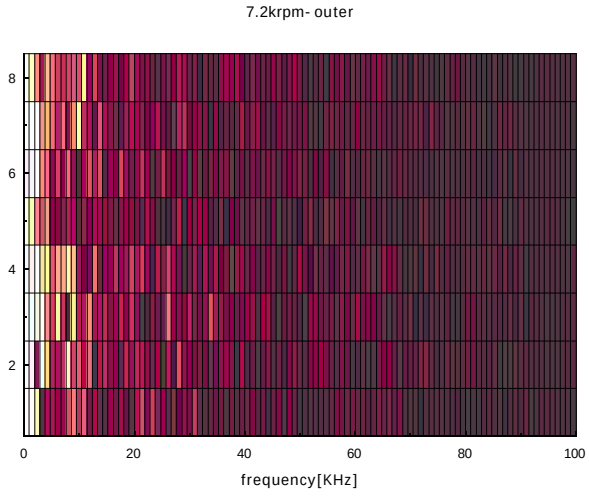

Fig. 3.3.10 FFT analysis of outer line modulation for each 45 deg segment.

[Un-textured disk at 5400rpm]

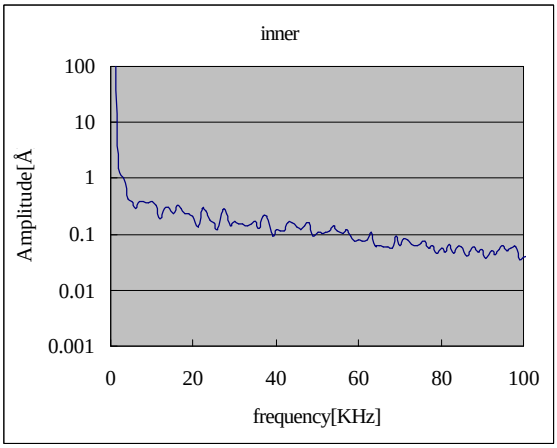

Fig. 3.3.11 FFT analysis of inner line modulation for the full circle.

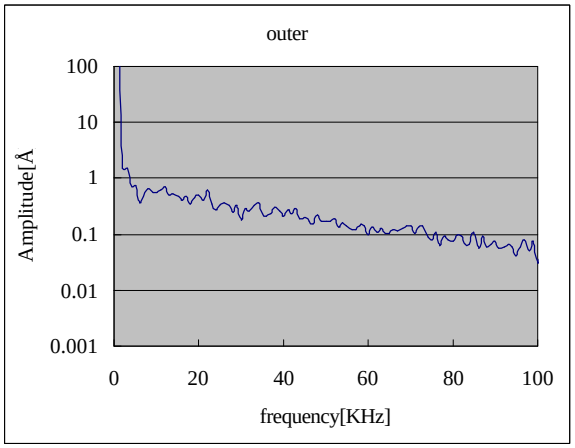

Fig. 3.3.12 FFT analysis of outer line modulation for the full circle.

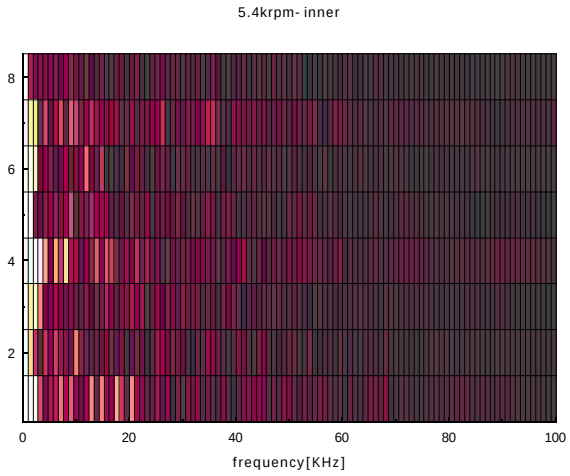

Fig. 3.3.13 FFT analysis of inner line modulation for each 45 deg segment.

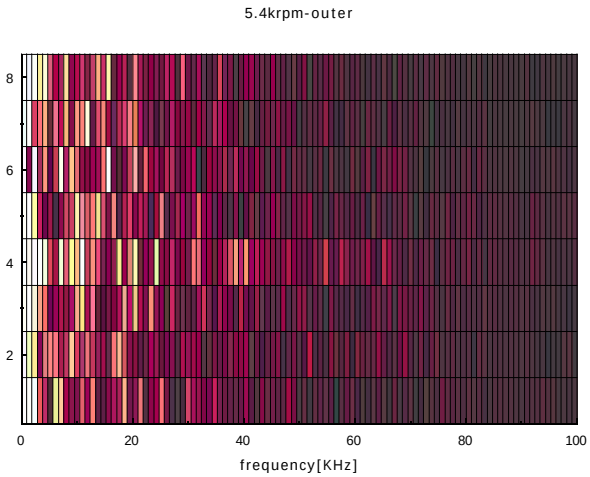

Fig. 3.3.14 FFT analysis of outer line modulation for each 45 deg segment.

[textured disk at 7200rpm]

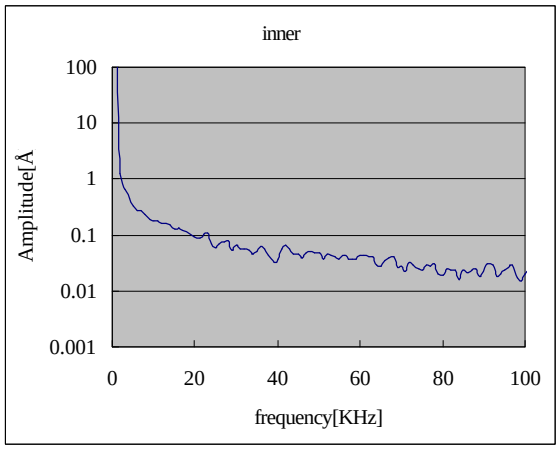

Fig. 3.3.15 FFT analysis of inner line modulation for the full circle.

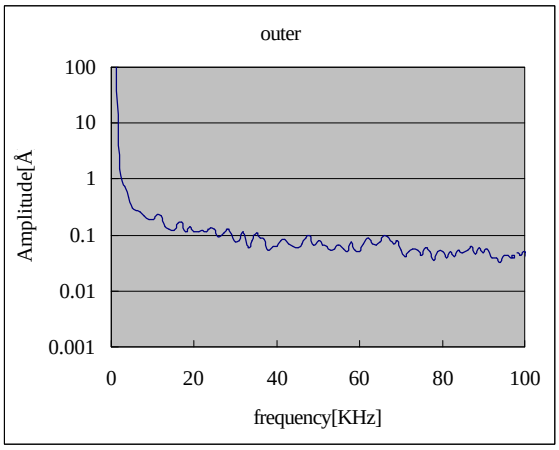

Fig. 3.3.16 FFT analysis of outer line modulation for the full circle.

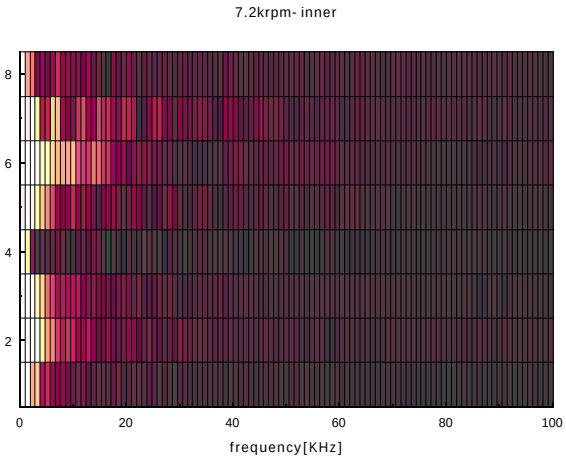

Fig. 3.3.17 The FFT analysis result of inner line modulation (FFT analysis of each 45[deg] area)

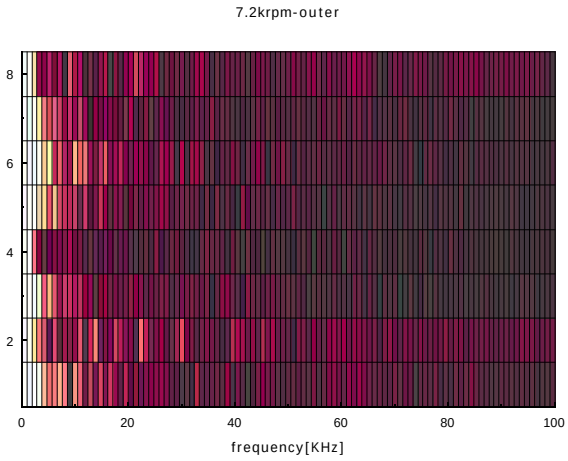

Fig. 3.3.18 The FFT analysis result of outer line modulation (FFT analysis of each 45[deg] area)

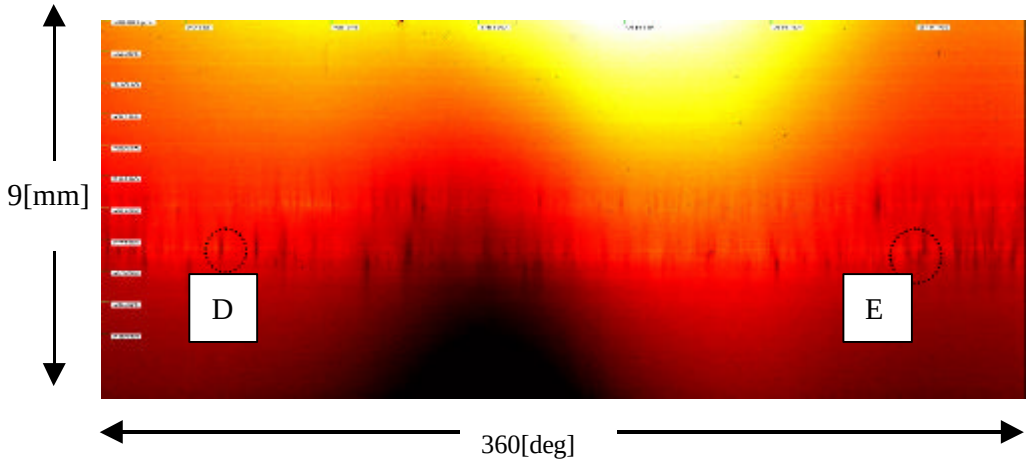

Fig. 3.3.19 Disk surface after a long-term flyability test of 70 hours

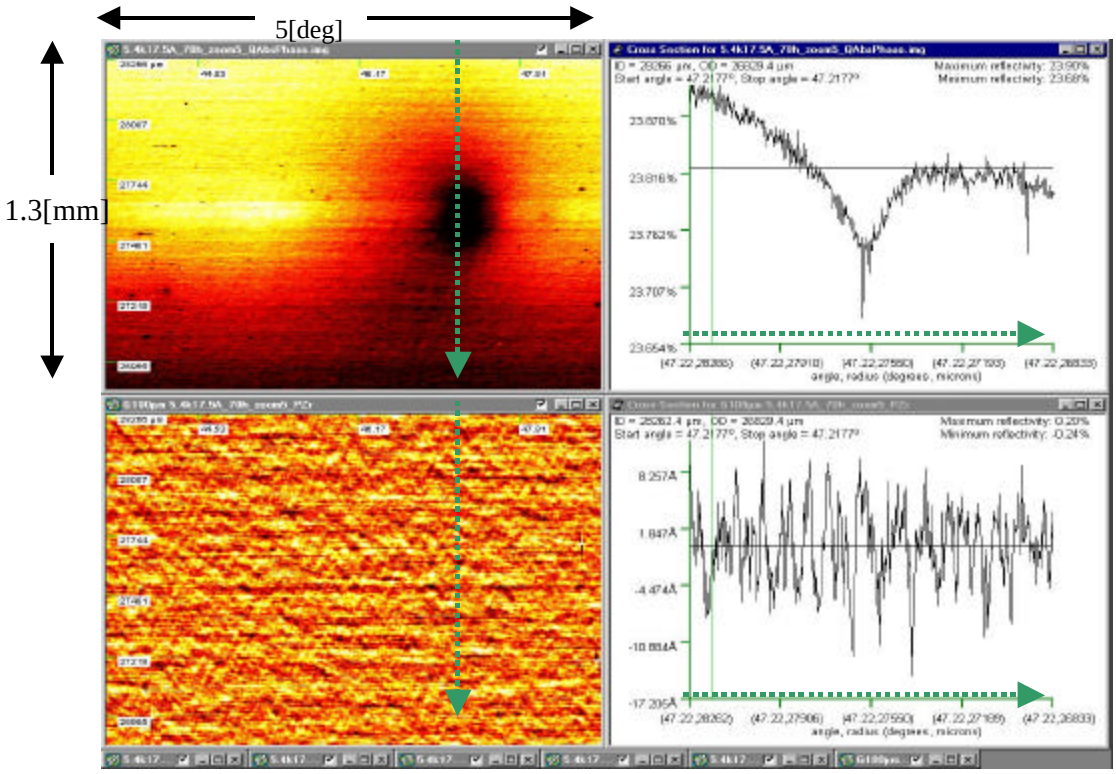

Fig. 3.3.20 Detail of position “D” in Fig. 3.3.19
(upper left) Phase-shift image
(upper right) Cross section profile of the Phase-shift image
(lower left) Topography image
(lower right) Cross section profile of the Topography image

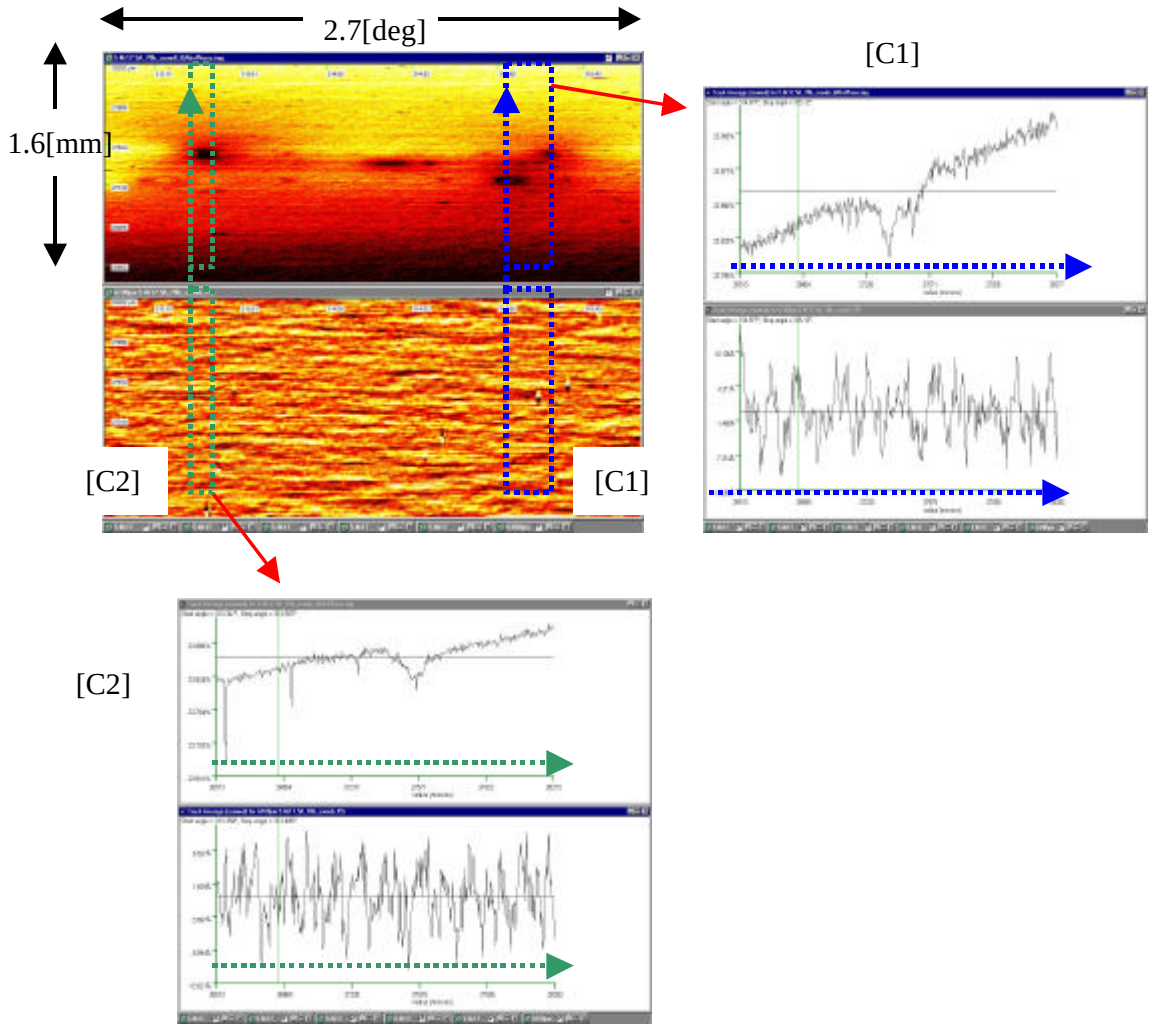

Fig. 3.3.21 Detail of position “E” in Fig. 3.3.19
(upper left) Phase-shift & Topography images
(upper right) Cross section profile of “C-1”
(lower left) Cross section profile of “C-2”